Preparation of pickering emulsion of cinnamon essential oil using soybean protein isolate-chitosan particles as stabilizers

Zijun WU[1], Jie YAN[2]* , Zhijian ZHOU[2], Qiulin XU[2], Qiaoguang LI[2]* , Guangqing LI[2], Xigui LI[3], Xitong FANG[2], QiuLing ZHONG[1]

Abstract

This study presents the preparation of cinnamon essential oil Pickering emulsion, aiming to improve the physicochemical properties, water sol ubility, and emulsion stability of cinnamon essential oil. The oil-in-water Pickering emulsion was prepared by ultrasonic emulsification, in which SPICS (soybean protein isolate (SPI)-chitosan (CS) composite granule) was used as the wall material and cinnamon essential oil was used as the core material. The emulsification performance of SPICS was evaluated, and the stability of Pickering emulsion was tested. The results showed that there was hydrogen bonding between SPI and CS, and the tertiary structure of SPI was change, which enhances the hydrophobicity of SPICS surface. When the mass ratio of SPI to CS was 14:1, the emulsification activity of SPICS was 71.92 m^2g^{-1} and its emulsion stability was 106.29%; it also had good dispersibility in water. When the volume of the oil phase was 60%, the encapsulation rate of cinnamon essential oil was 65.23%, the Pickering emulsion did not show obvious delamination for one month; and rheological tests showed the presence of shear thinning, which was judged to be a pseudoplastic fluid. Therefore, SPICS can be used as a wall material to prepare Pickering emulsion of cinnamon essential oil with good stability.

Keywords: Pickering emulsion; soybean protein isolate-chitosan particles; stability.

Practical Application: Preparation of cinnamon essential oil Pickering emulsion.

1 Introduction

Cinnamon essential oil can be extracted from some parts of cassia tree. Its main active ingredients include trans-cinnamaldehyde and trans-cinnamic acid, which are the compounds that have antioxidant activity, antibacterial, anti-inflammatory, and anti-tumor effects (Al-Nabulsi et al., 2020; Mahmoudzadeh et al., 2022). However, cinnamon essential oil has poor water solubility, low volatility, and poor stability, thus has limited application. Scholars have explored some applications of essential oils in the form of microcapsules, composites, microemulsions, etc (Hojatoleslami et al., 2022; Karimi Sani et al., 2020; Tamošaitis et al., 2022), At present, most cinnamon essential oil is embedded in microcapsules (Li et al., 2020). Researchers mainly use starch (Cao et al., 2022), gum Arabic (Fu et al., 2022), cyclodextrin (El Kharraf et al., 2021), and other polysaccharides as wall materials for cinnamon essential oil microcapsules. The preparation methods of microcapsules mainly include the homogeneous emulsification method, co-precipitation method, and coacervation method, among other methods. These processes are complicated; and some of them also adopt the spray-drying method, which can affect the active ingredients of essential oil due to high temperatures (Guo et al., 2020). As a countermeasure to overcome this problem, cinnamon essential oil has been embedded in the form of oil-in-water Pickering emulsion (Horvath et al., 2018).

Pickering emulsions use solid particles as stabilizers, and the currently used stabilizers consist of proteins, polysaccharides, or protein-polysaccharide complexes (Cao et al., 2020; Yi et al., 2021). Proteins and polysaccharides are combined to form a new biomolecular complex that has the properties of both proteins and polysaccharides, which is more advantageous than single proteins or single polysaccharides.

Protein solid particles that are mainly used in Pickering emulsion include SPI (Zhang et al., 2022), whey isolates protein (Qin et al., 2022), zein (Li et al., 2021b), and wheat gliadin (Zhu et al., 2021). Alcohol-soluble proteins need to be treated by an anti-solvent method prior to the further application in emulsions (Liu et al., 2021). Compared with animal proteins, plant proteins can be obtained at a lower cost. SPI has a high protein content and various functions, such as emulsification, water absorption, gelation, and foaming functions (Lu et al., 2022). It has been reported that proper sonication can improve the spatial structure of SPI and promote its binding to soybean soluble polysaccharides (Ding et al., 2018). Moreover, pH 3 has been reported to be favorable for enhancing the gelation of SPI during sonication (Cai et al., 2021). CS is a polysaccharide polymer material widely found in nature. It is non-toxic and easily biodegradable and has good compatibility, strong antibacterial property, and good adsorption performance

(Barrera-Ruiz et al., 2020). Studies have shown that SPI can form a complex with CS through electrostatic interaction, and the average particle size of the complex increased significantly (Wu et al., 2018a). A complex of SPI and CS has been successfully used to prepare oil-in-water Pickering emulsion, and the emulsion is stable at a wide ionic strength range and a wide temperature range (0-60 °C); nonetheless, the composite ratio of SPI and CS was not discussed in the paper (Yang et al., 2020).

In this study, SPICS was first prepared using SPI and CS as raw materials, and an O/W Pickering emulsion with good stability was prepared using the SPICS solution as the aqueous phase and cinnamon essential oil as the oil phase. The effects of SPI:CS ratios on the emulsification performance of SPICS were investigated by means of emulsification characteristics, average particle size, polydispersity index (PDI), etc. Further, the Pickering emulsions containing cinnamon essential oil at different volume fractions were prepared by ultrasonic emulsification. Physical stability, droplet size, and encapsulation efficiency of the emulsion were studied during storage. The main workflow is shown in Figure 1.

2 Materials and methods

2.1 Materials

SPI was purchased from Linyi Shansong Biological Products Co. Ltd., Shandong, China. CS was purchased from Sinopharm Chemical Reagent Co. Ltd., Cinnamon essential oil was purchased from Luoding Yuelong Industrial Co. Ltd., Guangdong, China. SDS, glacial acetic acid, and ethanol were purchased from Damao Chemical Reagent Factory. All other chemicals were of analytical grade and deionized water was used throughout.

2.2 Preparation of SPICS

SPICS was prepared following a previously described method with minor modifications (Ding et al., 2017b). In the preparation of an SPI solution (20 mg·mL⁻¹), SPI (10.00 g) was dispersed in 500 mL of deionized water, magnetically stirred at ambient temperature for 2 h, and then ultrasonicated at 400 W and 25 °C for 15 min (Bilon-10000D, Bilon Instrument Co., Ltd., Shanghai, China). CS (1.00 g) was dispersed in 50 mL of acetic acid solution at pH 3 and magnetically stirred at ambient temperature for 4 h to obtain a CS solution (20 mg·mL⁻¹).

The SPI solution was mixed with the CS solution at ratios of 5:1, 8:1, 11:1, 14:1, 17:1, and 20:1 (v/v). After their pH was adjusted to pH 3.0 with HCl (0.1 mol·L⁻¹), the mixtures were then freeze-dried to a constant weight to obtain products named SPICS-5, SPICS-8, SPICS-11, SPICS-14, SPICS-17, and SPICS-20, respectively.

2.3 Characterization of SPICS

Fourier transform-infrared spectroscopy (FT-IR)

The samples were mixed with KBr, pressed into tablets, and then scanned on a Fourier transform infrared spectrophotometer (Spectrum 100, Perkin Elmer, UK) at a frequency range of 4000-400 cm⁻¹; KBr was used to obtain the background signal.

Particle size and zeta potential

Samples (10 mg each) were dispersed in 10 mL of deionized water and then sonicated for 20 min until the particles were uniformly dispersed. Each sample (2-3 mL) was then transferred to a cuvette (light path range = 1 cm) and then subjected to particle size and potential measurements using a dynamic light scattering nanoparticle size analyzer (NanoBrook90Plus PALS, Brookhaven Instruments, Inc., USA).

Fluorescence intensity

The fluorescence of the samples was determined on a hybrid multi-mode microplate reader (Synergy H1, Agilent Technologies,
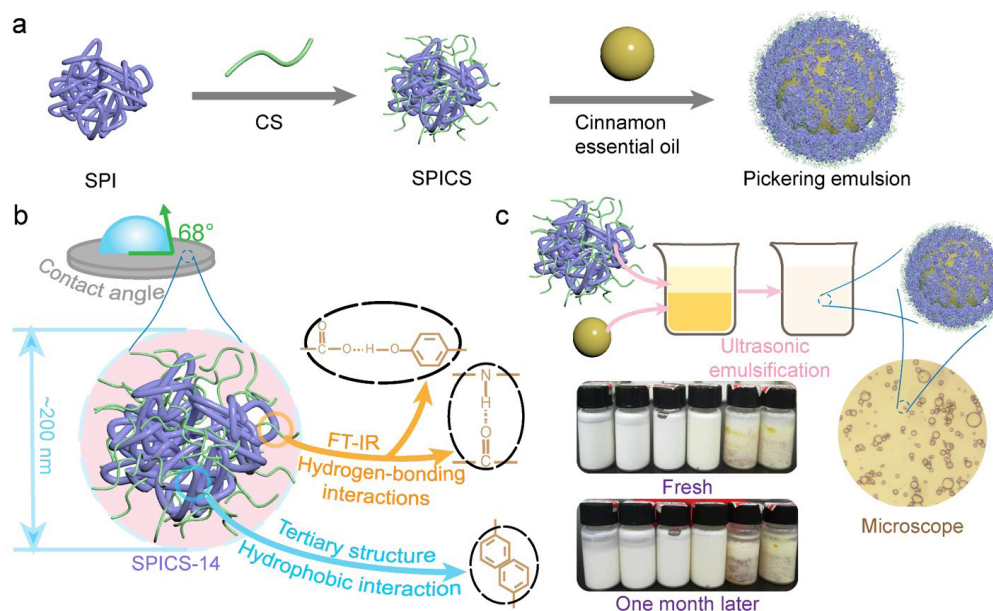

Figure 1. (a) Main Workflow; (b) Formation principle of SPICS; (c) Emulsion formation path.

USA) using 1-anilinonaphthalene-8-sulfonic acid ammonium (ANS) as a probe. The measurement was carried out at an excitation wavelength of 350 nm and an emission wavelength of 460 nm. The sample concentration was 5 mg·mL^{-1}.

Determination of particle wettability

The samples were pressed into thin slices with a size of about 2 mm using a tableting machine. After that, they were placed on a test bench, and water was dripped on their surface using an injector. The water contact angle was measured using an optical contact angle meter (DSA100, KRÜSS, Hamburg, Germany).

Determination of emulsifying properties

The determination was conducted as described previously with slight modifications (Song et al., 2018). SPICS solution (16 mL, 20 mg·mL^{-1}) was mixed with cinnamon essential oil (4 mL) in a 25-mL beaker, magnetically stirred, and then ultrasonicated at 400 W for 2 min. Immediately after that, fresh emulsion (100 μL) at the bottom was withdrawn using a 100-μL pipette and then placed in a 10-mL volumetric flask. Its volume was adjusted with 0.1% SDS, and its absorbance at 500 nm was measured using an ultraviolet spectrophotometer (UV-6100, Shanghai Mapada Instruments Co., Ltd., China); 0.1% SDS solution was used as a blank control. The emulsion was let stand for 10 min, and the above steps were repeated. For comparative tests, the SPICS solution was replaced with SPI solution. The emulsification property of SPICS including the emulsification activity index (EAI) and emulsion stability index (ESI) were calculated using Equations 1 and 2 (Nakamura et al., 2004), respectively.

$$EAI\,(m^2 \cdot g^{-1}) = \frac{2\,x\,2.303}{c\,x\,\varphi Lx10^4}\,X\,A_0\,X\,D \qquad (1)$$

$$ESI\,/\,\% = \frac{A_{10}}{A_0} \times 100\% \qquad (2)$$

where: c (g·mL^{-1}) is the mass concentration of SPICS (at different ratios) or SPI solution, c = 0.02; φ is the volume fraction of the oil phase in the emulsion, φ = 0.2; L is the cuvette light path range, cm; D is the dilution factor of 1000; and A_0 and A_{10} are the absorbance at 500 nm at 0 and 10 min, respectively.

2.4 Preparation of cinnamon essential oil Pickering emulsion

The Pickering emulsion was prepared by ultrasonic emulsification (Wu et al., 2018b). An aqueous solution of SPICS-14 (1%) was mixed with cinnamon essential oil at ratios of 3:7, 4:6, 5:5, 6:4, 6.5:3.5, and 7:3 (v/v). Each mixture was then treated with pulsed ultrasound (Bilon-10000D, Bilon Instruments Ltd., Shanghai, China; ultrasonic power = 400 W, pulse time = 1.0 s, and intermittent time = 1.2 s) for 44 min to obtain Pickering emulsion. The emulsions were named as P-30, P-40, P-50, P-60, P-65, and P-70 according to the volumes of the oil phase in the emulsion.

2.5 Characterization of Pickering emulsion

Stability test

Storage stability: 5 mL of Pickering emulsion was placed in a colorless transparent glass bottle. The appearance of the emulsion was observed and recorded on days 1, 3, 7, 15, and 32.

Centrifugal stability: 5 mL of cinnamon essential oil Pickering emulsion was placed in a centrifuge tube, and its total height was recorded. After that, the emulsion was centrifuged at different speeds (4000 rpm, 6000 rpm, 8000 rpm, 10000 rpm, or 12000 rpm), each for 10 min using a table-type high-speed laboratory centrifuge (H/T20MM, Hunan Herexi Instrument & Equipment Co., Ltd, China). The height of the water layer was recorded (if the liquid surface was tilted after centrifugation, the heights on both sides were measured and the values were averaged). The creaming index (CI) of emulsion was calculated using Equation 3 (Li et al., 2019):

$$CI\,/\,\% = \frac{Hs}{Ht}\,X\,100 \qquad (3)$$

where Hs (cm) is the height of the water layer and Ht (cm) is the total height of the emulsion.

Thermal stability: the thermal stability of the emulsions was determined using a thermogravimetric analyzer (TGA2, Mettler-Toledo, Switzerland) at temperatures from 40-400 °C at a heating rate of 10 °C/min^{-1} under nitrogen at 10 mL·min^{-1}.

Observation of micromorphology

The microscopic morphology of the emulsions was observed using a metallographic microscope (MIT500, Chongqing Optec Instrument Co., Ltd, China). Pickering emulsion (100 μL) was diluted in 1.00 mL of deionized water, placed on a glass slide, and then covered with a coverslip. After amplification for 400 times, the microscopic morphology of the emulsion was observed.

Particle size and potential

Pickering emulsion (10 μL) was diluted 1000 times in deionized water and ultrasonically dispersed for 20 min; and ~2-3 mL of the dispersion was then transferred to a plastic cuvette. The test was carried out using a dynamic light scattering nanoparticle analyzer (NanoBrook90Plus PALS, Brookhaven Instruments Co., Ltd. USA)

Rheological properties

An emulsion sample (~17-18 mL) was placed on the concentric barrel fixture of a rheometer (Viscotester iQ, Thermo Fisher Scientific, USA), whereby it was preserved at 25 °C for 2 min and sheared at 10 to 100 s^{-1} to obtain the viscosity and stress curves.

Encapsulation efficiency

The determination of encapsulation efficiency was slightly improved from the method reported in the literature (Hu & McClements, 2015).

Wavelength selection and construction of a standard curve for cinnamon essential oil: an anhydrous ethanol solution of cinnamon essential oil was scanned from 200 to 600 nm on an ultraviolet spectrophotometer (UV-6100, Shanghai Mapada Instruments Co., Ltd., China); the maximum absorbance of the emulsion was 286 nm. An absorbance at 286 nm of cinnamon essential oil at various concentrations (0.87, 1.74, 2.61, 3.48, 4.35, and 5.22 µg·mL^{-1}) was measured. The standard curve was plotted, and the curve was linear with the linear regression equation: $y = 0.1596x + 0.0091$, $R^2=0.99955$ (where: y is the absorbance at 286 nm of the sample; and x is the mass concentration of cinnamon essential oil in anhydrous ethanol solution, µg·mL^{-1}).

Determination of free cinnamon essential oil in emulsion: 0.2 mg of Pickering emulsion was mixed with 8 mL of anhydrous ethanol and then let stand for 5 min; after that, the mixture was centrifuged at 12000 rpm for 15 min. An absorbance at 286 nm of the supernatant was measured. The mass concentration of free cinnamon essential oil in the emulsion was calculated using the formula obtained from the standard curve described above.

Determination of cinnamon essential oil extracted from emulsion by ultrasonic extraction: The Pickering emulsion in anhydrous ethanol was subjected to ultrasonic treatment at 50 °C and 400W for 4 min. Other steps were the same as those described in the "determination of free cinnamon essential oil in emulsion", extracted from emulsion by ultrasonic extraction. The encapsulation efficiency (EE) of cinnamon essential oil in the emulsion was calculated by Equation 4.

$$EE / \% = \frac{A - B}{C} \times 100 \qquad (4)$$

where A (mg·mL^{-1}) is the mass concentration of ultrasonically extracted cinnamon essential oil, B (mg·mL^{-1}) is the mass concentration of free cinnamon essential oil in the emulsion, and C (mg·mL^{-1}) is the total mass concentration of cinnamon essential oil in the emulsion.

2.6 Statistical analysis

Data are expressed as mean ± standard deviation of at least three repeated measurements. IBM SPSS version 26 was used to determine the significant difference and Origin 9.1 software was used for statistical analysis.

3 Results and discussion
3.1 Characteristics of SPICS

FT-IR spectra

Figure 2a shows the FT-IR spectra of SPI, CS, and SPICS. As can be seen, SPI exhibited a wide characteristic peak at 3284 cm^{-1} attributed to the stretching vibration peak of free hydroxyl, carboxyl, and amino after molecule association of protein. The absorption peaks at 1642 cm^{-1} and 1529 cm^{-1} can be assigned to the stretching vibration of amide *I* (with a free carbonyl group) and the bending vibration of amide *II* (with an amino group), respectively (Zhou et al., 2020). The absorbance peak of CS at 1607 cm^{-1} is attributed to free carbonyl group in amide *I* and the bending vibration of amide *III* (with an amino group). The absorbance peak at 1069 cm^{-1} is the stretching vibration absorption peak of C-O bond in CH-OH. The infrared spectra of SPICS exhibited the characteristic peaks of SPI and CS. SPICS also exhibited a wide and strong absorption band near 3388 cm^{-1}. Compared with that at 3284 cm^{-1} of SPI, the absorption band of SPICS was shifted to a higher wavenumber. The change of peak position indicates that hydrogen bonds were formed between SPI and CS (Sun et al., 2017). Compared with the peak positions of SPI and CS amide bands, the peaks were shifted from 1642 cm^{-1} and 1607 cm^{-1} to 1659 cm^{-1} and from 1529 cm^{-1} to 1538 cm^{-1}, which suggests that there were electrostatic interactions between the carboxyl group in SPI and the amino group in CS (Mauricio-Sánchez et al., 2018; Li et al., 2021a). Together, SPI and CS were combined to generate SPICS through hydrogen bonds and electrostatic forces.

Particle size and zeta potential

The particle size distribution of SPICS and SPI is shown in Figure 2b, and the corresponding values are tabulated in Table 1.
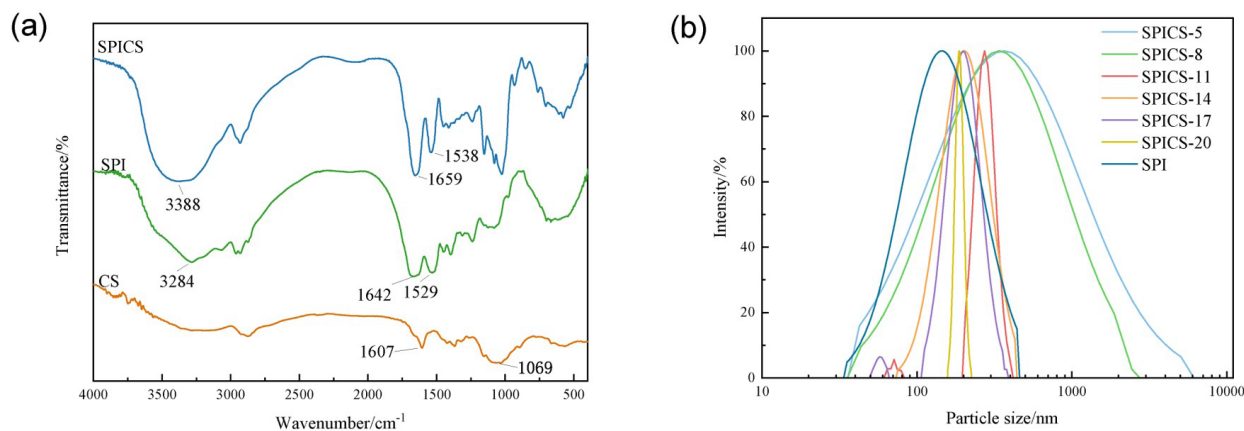

Figure 2. (a) FT-IR spectra of SPICS, SPI, and CS; (b) Particle size distribution of SPICS and SPI.

The data showed that the APS of SPI was 129.15 ± 2.15 nm. At V_{SPI}/V_{CS} = 20/1, the APS of SPICS was 179.73 ± 1.42 nm. With increasing CS proportion, the APS of SPICS had an increasing trend. At V_{SPI}/V_{CS} = 5/1, the APS of SPICS was increased to 295.69 ± 16.86 nm, indicating that the presence of both SPI and CS allows for a larger complex size. This result is similar to what is speculated in the literature (Li et al., 2021a).

It has been reported that smaller particles can more quickly and accurately adsorb the oil-in-water interface, and the filling degree of the interface is also larger, resulting in more stable Pickering emulsions (Matos et al., 2017). Although CS or SPI alone has small particle sizes, CS can allow for stronger water absorption. However, it needs hydrophobic modification prior to being used as a solid particle stabilizer for Pickering emulsion. Additionally, SPI can be easily disintegrated by environmental factors; thus, it needs to be modified by some physical and chemical methods to obtain a more stable Pickering emulsion (Li et al., 2018). The synergistic effect of protein and polysaccharide allows for good properties of the emulsion (Jafaria et al., 2020).

As shown in Figure 2b and Table 1, the particle size distribution of SPICS-5 and SPICS-8 were very wide ranging from 42 to 5058 nm and 43 to 2435 nm, respectively. Their PDI values were close to 0.3, and their APS were 295.69 ± 16.86 nm and 293.45 ± 13.74 nm, respectively, which is indicative of particle agglomeration. The particles with sizes below 50 nm are CS molecules unbound to SPI. SPICS-14, SPICS-17, and SPICS-20 had smaller particle sizes of 202.12 ± 12.37 nm, 180.40 ± 5.16 nm, and 179.73 ± 1.42 nm, respectively. However, homogeneity of the particles also has a certain effect on the formation of emulsions. SPICS-14 had a low PDI of 0.147 ± 0.040, indicating that it has good uniformity.

Table 1 shows that SPICS had negative potentials with values ranging from -57 mV to -58.5 mV; and the overall variation was negligible. The zeta potential value can indicate the stability of solid particles (Jiang et al., 2018). That is, the absolute zeta potential values of <10 mV, 10-20 mV, 20-30 mV, and >30mV are indications that the dispersion systems are highly unstable, relatively stable, moderately stable, and highly stable, respectively (Agrawal & Patel, 2011). SPICS had the absolute zeta potential values between 57 and 58 mV, indicating that they have high stability.

Fluorescence intensity

The fluorescence intensity of each sample is shown in Figure 3a. The fluorescence intensity of SPI was 500369 RFU,

Table 1 Average particle size (APS), polydispersity coefficient (PDI), and electric potential of SPICS and SPI.

Sample	APS/nm	PDI	Zeta/mV
SPICS-5	295.69 ± 16.86[a]	0.292 ± 0.051	-57.39 ± 0.20
SPICS-8	293.45 ± 13.74[a]	0.281 ± 0.036	-58.34 ± 0.15
SPICS-11	236.99 ± 1.84[b]	0.214 ± 0.019	-57.51 ± 0.29
SPICS-14	202.12 ± 12.37[c]	0.147 ± 0.040	-57.18 ± 0.09
SPICS-17	180.40 ± 5.16[d]	0.172 ± 0.028	-57.41 ± 0.26
SPICS-20	179.73 ± 1.42[d]	0.482 ± 0.564	-57.94 ± 0.13
SPI	129.15 ± 2.15[e]	0.221 ± 0.015	-38.35 ± 0.08

Different letters within the same row indicate the significant difference (p < 0.05).

while that of SPICS was above 1.4×10^6 RFU. Figure 3a also shows that with the increase of SPI content, the fluorescence intensity of SPICS gradually increased until reaching the maximum value (at SPICS-14), and then decreased. ANS interacts with hydrophobic groups on the surface of protein to produce fluorescence; thus, the fluorescence intensity can reflect the hydrophobicity of protein (He & Wang, 2018). This shows that under the action of CS, the hydrophobic groups of SPI become exposed, causing its surface hydrophobicity to be significantly enhanced.

As shown in Figure 3a, with the increase of SPI content, the hydrophobicity of SPICS first increased and then decreased. This observation might be related to the structural form of SPI molecule. SPI has a dense spherical or ellipsoidal solid structure containing hydrophobic side chains embedded inside the structure and hydrophilic side chains exposed to the surface (Hu & Li, 2021). After interacting with CS, the interior structure of SPI may become exposed, causing its hydrophobicity to increase; the higher the SPI concentration, the higher the degree of exposure of the hydrophobic side chains. When the concentration of SPI was too high, the numbers of hydrophobic groups that were exposed were also high. This can lead to excessive hydrophobic interactions, causing the particles to become aggregated. As a result, the proportion of surface hydrophobic groups and the surface hydrophobicity of SPI were reduced.

According to the literature, the sizes of protein aggregates are believed to affect the hydrophobicity of protein (Jiang et al., 2018). While small aggregates have high hydrophobicity, large aggregates, in which spatial steric hindrance can be generated, have low hydrophobicity (Ding et al., 2017a). In this paper, the amount of SPI was high, whereas that of CS was relatively low. As described in Section 3.1, hydrogen bonds and electrostatic interactions were formed between SPI and CS. These forces and the bridging effect of a small amount of CS caused SPI to form aggregates. When the SPI content was low, the aggregates were small and the hydrophobicity was high. By contrast, when the SPI content was very high, the aggregates were very large and the hydrophobicity was low. The variation of hydrophobicity of SPICS with increasing SPI content also followed the same trend.

Contact angle

As shown in Figures 3b and 3c, the contact angle for each solid particle could be ranked as follows: CS < SPICS < SPI < 90°. With contact angles of below 90°, the solid particles are more hydrophilic and suitable as solid stabilizers to emulsify the oil phase in oil-in-water Pickering emulsion (Albert et al., 2019) CS had the smallest contact angle of 49.18 ± 4.54°, whereas SPI had the largest contact angle of 84.33 ± 0.11°. Although their contact angles below 90° and their average particle sizes were low, neither CS nor SPI alone was suitable as a stabilizer for Pickering emulsions, as described in the part of Particle size and zeta potential. The contact angles of SPICS were between 57° and 69°; thus, it was suitable as a stabilizer for Pickering emulsions.

Figure 3b also shows that with the increase of SPI content, the contact angle of SPICS first increased and then decreased. The maximum contact angle of 68.505 ± 0.42° was reached when the mass ratio of SPI to CS was increased to 14:1. The contact
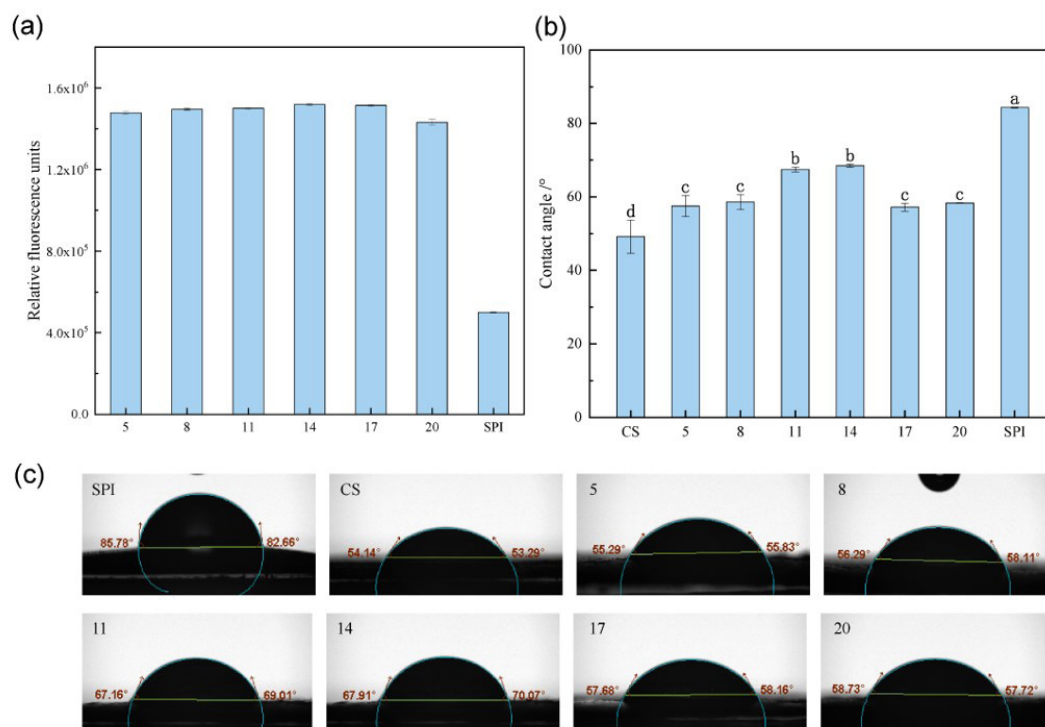
Figure 3. (a) Fluorescence intensity of SPICS and SPI; (b) Three-phase contact angles of SPI, CS, and SPICS; (c) Images showing contact angles for SPI, CS, and SPICS (5, 8, 11, 14, 17, and 20 refer to SPICS-5, SPICS-8, SPICS-11, SPICS-14, SPICS-17, and SPICS-20, respectively).

angle became smaller as the amount of SPI was continuously increased, and the contact angle of SPICS-20 was $58.33 \pm 0.11°$. Overall, the results showed that the hydrophobicity of SPICS first increased until reaching the highest value as the SPI dosage increased, and then decreased as the SPI dosage was further increased. This is consistent with the result described in Section Fluorescence intensity. For solid particles with the contact angle less than 90°: the larger the contact angle, the higher the hydrophobicity, the better the emulsification effect, and the higher the emulsion stability (Albert et al., 2019). Therefore, among all SPICS samples, SPICS-14 had the highest stability.

Emulsification properties

As can be seen in Figure 4, the emulsification activity (EAI) of SPICS ranged from 56.61 to 71.92 $m^2 \cdot g^{-1}$, which were greater than that of SPI (40.90 $m^2 \cdot g^{-1}$). With the increase of SPI content, the emulsifying activity of SPICS first increased until reaching the maximum value when the ratio of SPI to CS was 14:1; after that, it slowly decreased, which is consistent with the results on the effect of SPI content on the hydrophobicity of SPICS. As described above (regarding the effects of contact angle and fluorescence intensity on particle hydrophobicity), with the increase of SPI content, the hydrophobicity of SPICS increased; its properties were also closer to those of cinnamon essential oil, which allow for more SPICS to be adsorbed onto the oil-water interface to better prevent droplet aggregation, resulting in enhanced emulsifying activity. When the SPI concentration was too high, the hydrophobicity of SPICS drastically decreased.
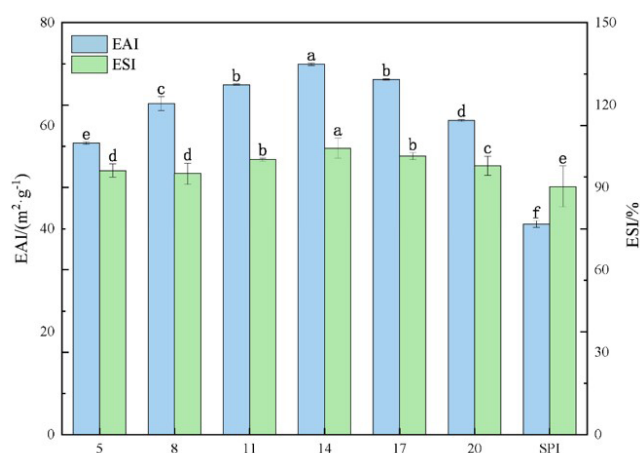

Figure 4. Emulsifying properties of SPICS and SPI (5, 8, 11, 14, 17, and 20 correspond to SPICS-5, SPICS-8, SPICS-11, SPICS-14, SPICS-17 and SPICS-20, respectively).

As a result, the properties of SPICS largely deviated from those of essential oil, which is not conducive to the arrangement of SPICS to the oil-water interface; thus, the emulsifying activity decreased.

Furthermore, according to the results on emulsion stability (ESI), the stability of SPI emulsion was 85.47%, which was lower than that of SPICS emulsion (94.32-106.29%). Despite a similar

trend, the overall variation of ESI was narrower than that of EAI. After using SPICS complex, the emulsion stability was improved. Taken together, the emulsifying activity and emulsifying stability data suggested that SPICS-14 had the highest emulsifying ability among all SPICS samples.

3.2 Performance of cinnamon essential oil Pickering emulsion

Storage stability

The emulsion stored at 4 °C is shown in Figure 5a. The Pickering emulsions prepared with different oil volume fractions (φ = 30%-60%) were uniform. When the oil phase ratio was more than 60%, emulsification appeared incomplete (this observation is not a part of our analysis and discussion). P-30, P-40, and P-50 had milky white colors, where P-60 had pale yellow color. After 3 days, water separation, stratification, and other appearances were not observed in the emulsion. A small amount of water emission of P-30 and P-40 was observed on day 7, and obvious stratification of water and emulsion was observed on day 30. The appearances of P-50 and P-60 were not significantly changed,

and the two samples were stable for one month. Water or oil separation did not occur within one month, an indication that the Pickering emulsion has good storage stability when the oil phase ratio was 50% or 60%.

Centrifugal stability

The stratification of the emulsion after high-speed centrifugation was similar to that reported in the literature (Wei & Huang, 2020). However, as can be seen from the appearance of P-65 and P-70 (Figure 5a) that the density of cinnamon essential oil was higher than that of water; thus, the emulsified layer was located above the oil layer. Figure 5b shows the creaming index of Pickering emulsion at different rotational speeds. With the increase of rotational speed, the creaming index shows an increasing trend. By comparison, the index of different oils had no obvious regularity when the centrifugal speed was below 8000 rpm; however, when the rotational speed was above 8000 rpm, the higher the oil content, the lower the index. The creaming index of P-30 increased to more than 50% because it had high water and SPICS contents, and the content of SPICS
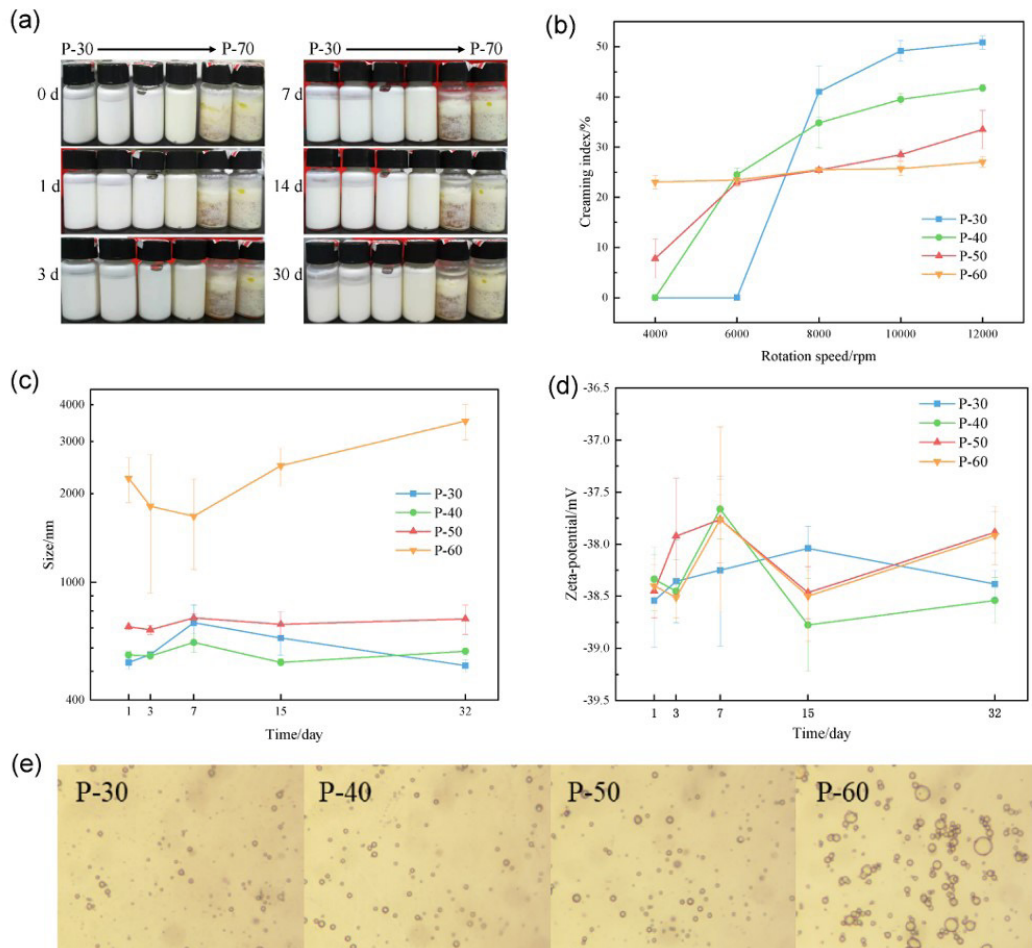

Figure 5. (a) Photographs of Pickering emulsion stored at 4 °C for 0, 1, 3, 7, 14, and 30 days and (b) creaming index of Pickering emulsion at different rotational speeds (at rotational speeds of 4000 r and 6000 r, the boundary of P-30 and P-40 was not obvious). Changes in particle size (c) and zeta-potential (d) of Pickering emulsion with storage time. (e) Microscopic images of different Pickering emulsion samples.

was sufficient to complete the adsorption in both water and oil phases. Therefore, a large amount of moisture was separated during high-speed centrifugation, causing the volume of the emulsion layer to decrease. The creaming index of P-60 was not significantly changed; it was stable at around 24.68% at a low centrifugal speed and increased to only 27.56% at 12000 rpm. This indicates that the P-60 emulsion is highly stable.

Particle size and potential of emulsion

Figure 5c shows the average particle size of Pickering emulsions containing oil phase at different volume fractions (φ = 30-60%) as a function of storage time. With increasing storage time up to one month, the Pickering emulsion with φ = 30-50% was only slightly changed, suggesting that it was relatively stable. The particle size of P-60 increased significantly, and agglomeration or demulsification was observed. This shows that SPICS plays a role in stabilizing the oil-water interface. When the amount of essential oil increases excessively to higher than the stabilization limit, the solid particles bridging droplets appear in the emulsion (Jiao et al., 2018), causing agglomeration or breakage of essential oil in the emulsion to occur. Observation of the Pickering microstructure (Figure 5e) showed that the size of P-60 was significantly larger than that of other emulsions, which is consistent with the results from particle size measurement shown in Figure 5c. The particle sizes of P-30 and P-40 were 530-600 nm, whereas those of P-50 were 700-800 nm and were relatively stable for one month. However, the particle size of P-60 increased from 2200 nm to 3300 nm as the storage time was prolonged. These results are similar to those reported in the literature (Yang et al., 2020), showing that after storing at 4 °C, the oil content and the droplet of the Pickering emulsion increased. As can be seen in Figure 5d, the potential of Pickering emulsions did not change significantly and were within a range of -38.5 mV to -37.8 mV over a month. This indicates that the emulsions have good stability.

Micromorphology of emulsion

The microstructures of Pickering emulsions containing oil phase at different volume fractions are shown in Figure 5e. The emulsion was uniformly dispersed in deionized water and appeared as spherical droplets. It could also be observed that SPICS formed an adsorption layer between the oil and water phases, and the adsorption layer was surrounded by ginger yellow oil droplets, the indication that the emulsion was an oil-in-water emulsion. Each emulsion was observed at the same magnification, and the droplet size of P-30, P-40, and P-50 (which was relatively uniform) was significantly smaller than that of P-60. This result is consistent with the results from particle size measurement. The number of solid particles was sufficient to stabilize all droplets, and the particles at the interface formed bridging flocculation with particles in the aqueous phase (Ding et al., 2018). Therefore, the emulsion was dispersed in water and became aggregated under a microscope; but it remained oil droplets.

Thermal stability

It can be seen that the heat loss of cinnamon essential oil had only one stage, and the maximum weight loss occurred at 171.35 °C. The heat loss of Pickering emulsion could be divided into two main stages. The first weight loss stage appeared at 70-80 °C. The weight loss in this stage was caused by evaporation of water, and the percent weight loss increased with the increase of water volume fraction. The second weight loss stage occurred at between 144 °C and 161 °C. The weight loss in this stage was caused by the thermal degradation of cinnamon essential oil in Pickering emulsion, and in contrast to the first stage, the percent weight loss decreased with the increase of water volume fraction. In addition, in the second weight loss peak in Figure 6b, the temperature decreased significantly with the decrease of cinnamon essential oil content. Combined with the results on emulsion microstructure, particle size, and emulsification index, we may conclude that the Pickering emulsions containing higher oil volume fractions have larger particle sizes and higher thermal degradation temperatures. Thus, P-60 had a larger particle size and higher oil content, and upon observing under a microscope, it contained more aggregates. In turn, the temperature required for thermal degradation of this sample was slightly higher, an indication that it is more stable under a thermal environment.

Rheological properties

Figures 6c and 6d show the changes in apparent viscosity and shear stress of Pickering emulsions with shear rate, respectively. According to Figure 5c, the viscosity of P-40, P-50, and P-60 emulsions was lower as the shear rate increased, which is indicative of shear thinning, suggesting that the emulsions belong to the pseudoplastic fluid. At the same time, their viscosity increased with the increase of oil phase content; the initial viscosity of P-40, P-50, and P-60 was 113.03 mPa·s, 406.95 mPa·s, and 987.01 mPa·s, respectively. For P-30 emulsion, there was no obvious regularity between viscosity and shear rate when the shear rate was less than 20 s^{-1}. However, when the shear rate was greater than 20 s^{-1}, the viscosity of this emulsion decreased slowly from 40.34 mPa·s to 33.42 mPa·s as the shear rate was increased. The magnitude of thinning was low, which might be due to the too low viscosity of the emulsion and the unobvious change trend. Figure 6d shows that there was no obvious regularity between the shear stress of P-30 and the shear rate when the shear rate was < 20 s^{-1}; except that, of which the shear stress increased and the viscosity decreased with increasing shear rate.

Emulsion encapsulation efficiency

Figure 7 shows the encapsulation rate of Pickering emulsion in encapsulating cinnamon essential oil. According to the figure, the encapsulation efficiency of emulsion increased with increasing essential oil content, and the encapsulation efficiency of P-60 was highest with a value of 65.23%. Theoretically, a low content of essential oil in the emulsion should sufficiently allow solid particles to be arranged at the oil-water interface, in turn increasing the encapsulation efficiency, which contradicts to the results from our experiment. One explanation for the observation can be that cinnamon essential oil has high volatility and certain solubility in water. The solubility of its main component, trans-cinnamaldehyde, is 1.1 g·L^{-1} on 20 °C (Rostiana et al., 2020). Ultrasonic emulsification, storage, and other operations may lead to certain losses of cinnamon essential oil. Combined with the
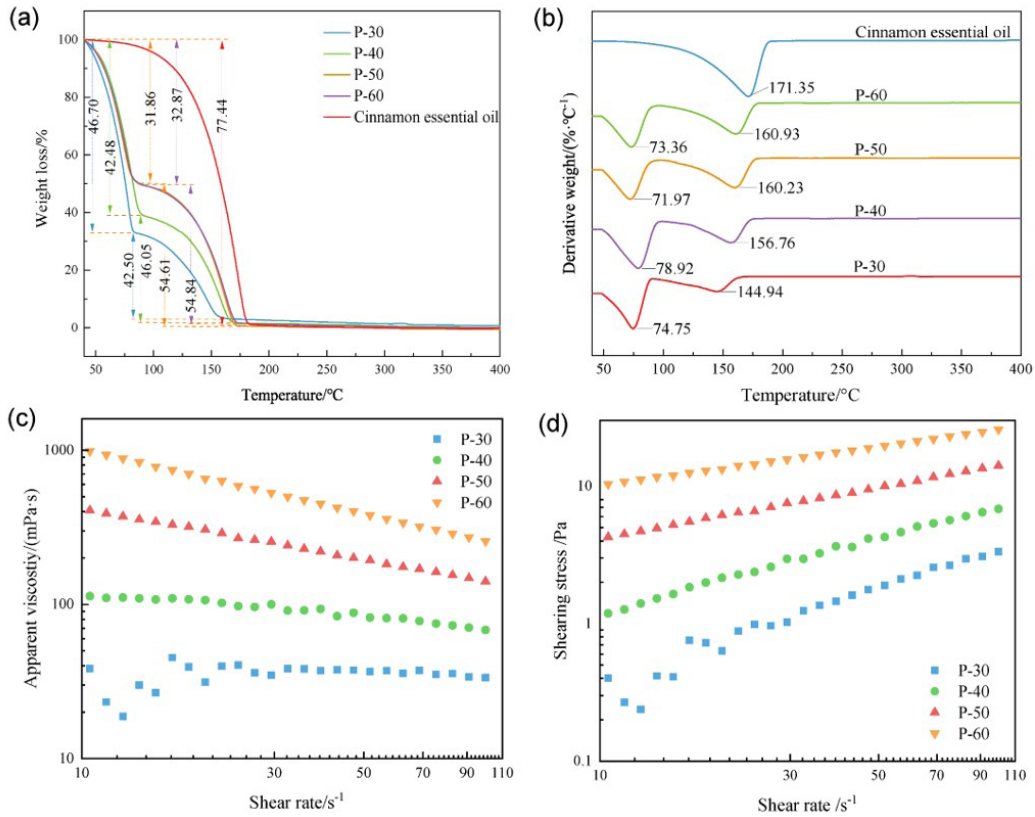
Figure 6. (a) TG and (b) DTG of Pickering emulsion and cinnamon essential oil. Changes in apparent viscosity (c) and stress variation (d) of Pickering emulsion as a function of shear rate.

results described in Sections Particle size and potential of emulsion and Micromorphology of emulsion, in which the particle size of P-30, P-40, and P-50 was found to be much smaller than that of P-60. In other words, the emulsion containing more water content likely has a higher contact angle between cinnamon essential oil and water. Thus, water can dissolve more cinnamon essential oil, resulting in a more serious loss of embedded essential oil, causing the encapsulation efficiency to reduce.

Meanwhile, according to the analysis described in Section Rheological properties, in which the viscosity of P-30, P-40, and P-50 was found to be much smaller than that of P-60; that is, the former had higher mobility than the latter. With high liquidity, contact areas with air, and volatility, some parts of the essential oil may be lost during storage, testing, and other operations, causing the encapsulation efficiency to be low. However, further research is needed to better justify this finding.

3.3 Analysis of the practical applications

SPICS complex has good emulsification ability, surface hydrophobicity, and particle dispersion, which can be used not only as a solid stabilizer to emulsify cinnamon essential oil, but also in other oil-in-water emulsion systems. It can be used to encapsulate other functional oil phases, such as deep-sea fish oil, camellia oil, flaxseed oil, etc., and can also be used to encapsulate and deliver oil-soluble drugs, such as curcumin, carotenoids,
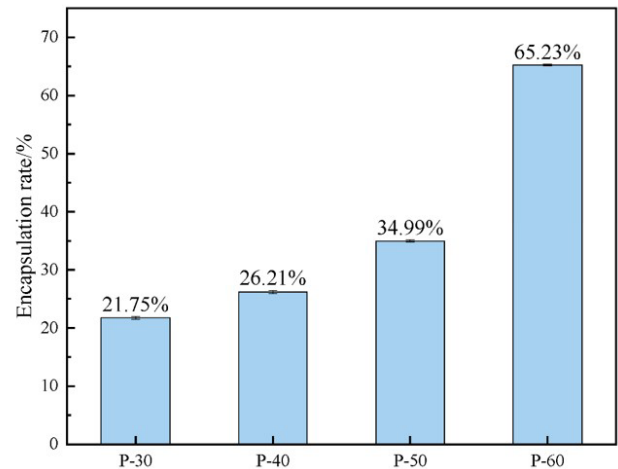

Figure 7. Encapsulation efficiency of Pickering emulsion in encapsulating cinnamon essential oil.

vitamin E, etc. The prepared Pickering emulsion of cinnamon essential oil has high stability can be maintained for more than one month, the encapsulation rate is up to 65.23%, and the droplet particle size distribution is narrow. These indicators can show that cinnamon essential oil can be well encapsulated, which can prevent the volatilization of essential oil and reduce

the loss; meanwhile the emulsion can be evenly dispersed in water and improve the bioavailability of cinnamon essential oil. In addition, cinnamon essential oil itself has certain antibacterial and antioxidant properties, so Pickering emulsion of cinnamon essential oil can be used as health care products or applied to food preservation, antibacterial and other food industry fields.

4 Conclusions

SPICS was prepared from SPI and CS at different mass ratios, and its emulsification, hydrophobicity, particle size distribution, and electrical potential were measured. The results showed that SPICS had high emulsification activity and emulsion stability, and its hydrophobicity was between that of SPI and CS. The particle sizes of SPICS ranged from 180 to 300 nm. With the increase of SPI content, the emulsifying properties and surface hydrophobicity of SPICS showed an increasing trend, followed by a decreasing trend. Among all SPICS samples, SPICS-14 had the best emulsification performance; its particle size was 202.12 ± 12.37 nm and its PDI was 0.147 ± 0.040.

SPICS-14 was selected to prepare cinnamon essential oil Pickering emulsion. The encapsulation efficiency of P-60 was 65.23%, the creaming index was 24.68%, and maintained below 30% within 30 days. P-50 and P-60 of the emulsions were left at 4 °C for more than 30 days without obvious delamination, indicating the formation of a stable oil-in-water Pickering emulsion. The analysis of rheological properties showed that Pickering emulsion had shear thinning phenomenon and was judged as pseudoplastic fluid.

References

Agrawal, Y. K., & Patel, V. R. (2011). Nanosuspension: An approach to enhance solubility of drugs. *Journal of Advanced Pharmaceutical Technology & Research*, 2(2), 81-87. http://dx.doi.org/10.4103/2231-4040.82950. PMid:22171298.

Albert, C., Beladjine, M., Tsapis, N., Fattal, E., Agnely, F., & Huang, N. (2019). Pickering emulsions: Preparation processes, key parameters governing their properties and potential for pharmaceutical applications. *Journal of Controlled Release*, 309, 302-332. http://dx.doi.org/10.1016/j.jconrel.2019.07.003. PMid:31295541.

Al-Nabulsi, A., Osaili, T., Olaimat, A., Almasri, W., Al-HOLY, M., Jaradat, Z., Ayyash, M., Awaisheh, S., & Holley, R. (2020). Inhibitory effect of thyme and cinnamon essential oils against *E. coli* O157:H7 in Tahini. *Food Science and Technology*, 40(4), 885-893. http://dx.doi.org/10.1590/fst.21619.

Hu, A., & Li, L. (2021). Effect mechanism of ultrasound pretreatment on fibrillation Kinetics, physicochemical properties and structure characteristics of soy protein isolate nanofibrils. *Ultrasonics Sonochemistry*, 78, 105741. http://dx.doi.org/10.1016/j.ultsonch.2021.105741. PMid:34537680.

Mauricio-Sánchez, R. A., Salazar, R., Luna-Bárcenas, J. G., & Mendoza-Galván, A. (2018). FTIR spectroscopy studies on the spontaneous neutralization of chitosan acetate films by moisture conditioning. *Vibrational Spectroscopy*, 94, 1-6. http://dx.doi.org/10.1016/j.vibspec.2017.10.005.

Barrera-Ruiz, D. G., Cuestas-Rosas, G. C., Sánchez-Mariñez, R. I., Álvarez-Ainza, M. L., Moreno-Ibarra, G. M., López-Meneses, A. K., Plascencia-Jatomea, M., & Cortez-Rocha, M. O. (2020). Antibacterial activity of essential oils encapsulated in chitosan nanoparticles. *Food Science and Technology*, 40(Suppl. 2), 568-573. http://dx.doi.org/10.1590/fst.34519.

Cai, S. K., Cui, Y. R., Qiu, T. T., Shi, Y., Shi, Y. H., Wang, Z. J., Zeng, M., & Chen, J. (2021). Effect of pH-ultrasonic treatment on gelation of soy protein isolate. *Shipin Yu Fajiao Gongye*, 47(24), 209-218. http://dx.doi.org/10.13995/j.cnki.11-1802/ts.028196.

Cao, J. Y., Xu, C., & Zhang, Z. (2022). Preparation and properties of modified porous starch embedded cinnamon essential oil and sodium metabisulfite microcapsules. *Journal of Food Science and Biotechnology*, 41(4), 74-83. http://dx.doi.org/10.3969/j.issn.1673-1689.2022.04.010.

Cao, Y. Q., Xiao, J. X., Jiang, L. H., & Huang, G. Q. (2020). Application of corn fiber in the preparation of pickering emulsions. *Journal of the Chinese Cereals and Oils Association*, 35(4), 54-60. http://dx.doi.org/10.3969/j.issn.1003-0174.2020.04.010.

Ding, J., Li, Y., Shi, B. R., Sun, H. B., Qi, B. K., & Jiang, L. Z. (2018). Freeze-thaw stability of emulsion system from ultrasound-modified soy protein isolate and soluble polysaccharide. *Shipin Kexue*, 39(9), 88-94. http://dx.doi.org/10.7506/spkx1002-6630-201809014.

Ding, J., Ma, W. J., Bi, S., Qi, B. K., Wang, Z. J., Sui, X. N., & Jiang, L. Z. (2017a). Effect of ultra-high pressure processing on the formation and stability of emulsions containing soy protein and soluble polysaccharide complexes. *Shipin Kexue*, 38(7), 96-101.

Ding, J., Qi, B., Jiang, N., Sui, X., Wang, Z., & Li, Y. (2017b). Structural properties of soybean protein isolate-chitosan complex treated by ultrasonic. *Nongye Jixie Xuebao*, 48(9), 352-358. http://dx.doi.org/10.6041/j.issn.1000-1298.2017.09.045.

El Kharraf, S., Farah, A., El Hadrami, E. M., El-Guendouz, S., Lourenco, J. P., Rosa Costa, A. M., & Miguel, M. G. (2021). Encapsulation of *Rosmarinus officinalis* essential oil in beta-cyclodextrins. *Journal of Food Processing and Preservation*, 45(10). http://dx.doi.org/10.1111/jfpp.15806.

Fu, L. X., Chen, M. M., Zhang, C. D., Li, D. W., Qian, L. L., & Zuo, F. (2022). Preparation and characterization of cinnamon-clove-thyme essential oil microcapsule. *Journal of the Chinese Cereals and Oils Association*, 37(2), 123-130. http://dx.doi.org/10.3969/j.issn.1003-0174.2022.02.020.

Guo, J., Li, P., Kong, L., & Xu, B. (2020). Microencapsulation of curcumin by spray drying and freeze drying. *Lebensmittel-Wissenschaft + Technologie*, 132, 109892. http://dx.doi.org/10.1016/j.lwt.2020.109892.

He, Q. J., & Wang, L. Q. (2018). Hydrophobicity analysis of soy protein in soybean water with different heating temperatures during painting and calligraphy restoration. *Chinese Journal of Analytical Chemistry*, 46(11), 1845-1850. http://dx.doi.org/10.11895/j.issn.0253-3820.171081.

Hojatoleslami, M., Ahari, H., Larijani, K., & Sharifan, A. (2022). Preservation effect of Lippia citriodora and Laurus nobilis nanoemulsions incorporated with polylactic acid composite film for rainbow trout fillet packaging. *Food Science and Technology*, 42, e83921. http://dx.doi.org/10.1590/fst.83921.

Horvath, B., Pal, S., & Szechenyi, A. (2018). Preparation and invitro diffusion study of essential oil Pickering emulsions stabilized by silica nanoparticles. *Flavour and Fragrance Journal*, 33(6), 385-396. http://dx.doi.org/10.1002/ffj.3463.

Hu, K., & McClements, D. J. (2015). Fabrication of biopolymer nanoparticles by antisolvent precipitation and electrostatic deposition: Zein-alginate core/shell nanoparticles. *Food Hydrocolloids*, 44, 101-108. http://dx.doi.org/10.1016/j.foodhyd.2014.09.015.

Jafaria, S. M., Doostb, A. S., Nasrabadic, M. N., Boostanid, S., & van der Meeren, P. (2020). Phytoparticles for the stabilization of Pickering emulsions in the formulation of novel food colloidal dispersions. *Trends in Food Science & Technology*, 98, 117-128. http://dx.doi.org/10.1016/j.tifs.2020.02.008.

Jiang, L., Chen, S., Li, Y., Wu, C., Wang, Z., Zhang, Q., Qi, B., Sui, X., Chen, F., & Xu, Z. (2018). Effects of complexation with anthocyanin on the structural and functional properties of denatured soybean protein. *Food Science*, 39(10), 20-27. http://dx.doi.org/10.7506/spkx1002-6630-201810004.

Jiao, B., Shi, A., Wang, Q., & Binks, B. P. (2018). High-internal-phase pickering emulsions stabilized solely by peanut-protein-isolate microgel particles with multiple potential applications. *Angewandte Chemie International Edition in English*, 57(30), 9274-9278. http://dx.doi.org/10.1002/anie.201801350. PMid:29845713.

Karimi Sani, I., Alizadeh Khaledabad, M., Pirsa, S., & Moghaddas Kia, E. (2020). Physico-chemical, organoleptic, antioxidative and release characteristics of flavoured yoghurt enriched with microencapsulated *Melissa officinalis* essential oil. *International Journal of Dairy Technology*, 73(3), 542-551. http://dx.doi.org/10.1111/1471-0307.12691.

Li, F. F., Li, X. H., Huang, K. L., Luo, Y. B., & Mei, X. H. (2021a). Preparation and characterization of pickering emulsion stabilized by hordein-chitosan complex particles. *Journal of Food Engineering*, 292, 110275. http://dx.doi.org/10.1016/j.jfoodeng.2020.110275.

Li, L., Zhang, W., Peng, J., Xue, B., Liu, Z., Luo, Z., Lu, D., & Zhao, X. (2020). A novel shell material-highland barley starch for microencapsulation of cinnamon essential oil with different preparation methods. *Materials*, 13(5), 1192. http://dx.doi.org/10.3390/ma13051192.

Li, M. F., He, Z. Y., Li, G. Y., Zeng, Q. Z., Su, D. X., Zhang, J. L., Wang, Q., Yuan, Y., & He, S. (2018). The formation and characterization of antioxidant pickering emulsions: effect of the interactions between gliadin and chitosan. *Food Hydrocolloids*, 90, 482-489. http://dx.doi.org/10.1016/j.foodhyd.2018.12.052.

Li, S., Li, C., Yang, Y. Z., He, X. W., Zhang, B., Fu, X., Tan, C. P., & Huang, Q. (2019). Starch granules as Pickering emulsifiers: Role of octenylsuccinylation and particle size. *Food Chemistry*, 283, 437-444. http://dx.doi.org/10.1016/j.foodchem.2019.01.020. PMid:30722895.

Li, W., Huang, D., Jiang, Y., Liu, Y., Li, F., Huang, Q., & Li, D. (2021b). Preparation of pickering emulsion stabilised by Zein/Grape seed proanthocyanidins binary composite. *International Journal of Food Science & Technology*, 56(8), 3763-3772. http://dx.doi.org/10.1111/ijfs.15067.

Liu, Q., Chang, X., Shan, Y., Fu, F. H., & Ding, S. H. (2021). Fabrication and characterization of Pickering emulsion gels stabilized by zein/pullulan complex colloidal particles. *Journal of the Science of Food and Agriculture*, 101(9), 3630-3643. http://dx.doi.org/10.1002/jsfa.10992. PMid:33275778.

Lu, S., Zhu, D., Bao, Y., Zhang, D., Hansong, Y., & Gu, C. (2022). Effect of covalent crosslinking of soybean protein isolate with genistein on protein characterization and structure. *Shipin Kexue*, 43(12), 94-100. http://dx.doi.org/10.7506/spkx1002-6630-20210706-051.

Mahmoudzadeh, P., Aliakbarlu, J., & Moradi, M. (2022). Preparation and antibacterial performance of cinnamon essential oil nanoemulsion on milk foodborne pathogens. *International Journal of Dairy Technology*, 75(1), 106-114. http://dx.doi.org/10.1111/1471-0307.12817.

Matos, M., Marefati, A., Bordes, R., Gutierrez, G., & Rayner, M. (2017). Combined emulsifying capacity of polysaccharide particles of different size and shape. *Carbohydrate Polymers*, 169, 127-138. http://dx.doi.org/10.1016/j.carbpol.2017.04.006. PMid:28504128.

Nakamura, A., Takahashi, T., Yoshida, R., Maeda, H., & Corredig, M. (2004). Emulsifying properties of soybean soluble polysaccharide. *Food Hydrocolloids*, 18(5), 795-803. http://dx.doi.org/10.1016/j.foodhyd.2003.12.005.

Qin, X. G., Yu, J. Y., Wang, Q., Zhang, H. Z., Chen, H. M., Hu, Z. Z., Lv, Q., & Liu, G. (2022). Preparation of camellia oil pickering emulsion stabilized by glycated whey protein isolate and chitooligosaccharide: Effect on interfacial behavior and emulsion stability. *Lebensmittel-Wissenschaft + Technologie*, 153, 112515. http://dx.doi.org/10.1016/j.lwt.2021.112515.

Rostiana, O., Suryani, E., Purwiyanti, S., Heriyanto, R., & Arlianti, T. (2020). Yield and essential oil quality of Indonesian ceylon cinnamon at different age of harvest. *IOP Conference Series. Earth and Environmental Science*, 418(1), 012025. http://dx.doi.org/10.1088/1755-1315/418/1/012025.

Song, C. L., Ren, J., Chen, J. P., Sun, X. H., Kopparapu, N. K., & Xue, Y. G. (2018). Effect of glycosylation and limited hydrolysis on structural and functional properties of soybean protein isolate. *Journal of Food Measurement and Characterization*, 12(4), 2946-2954. http://dx.doi.org/10.1007/s11694-018-9910-5.

Sun, C. X., Chen, S., Dai, L., & Gao, Y. X. (2017). Structural characterization and formation mechanism of zein-propylene glycol alginate binary complex induced by calcium ions. *Food Research International*, 100(Pt 2), 57-68. http://dx.doi.org/10.1016/j.foodres.2017.08.022. PMid:28888459.

Tamošaitis, A., JaruševičienÈ, A. È., StrykaitÈ, M., & Damašius, J. (2022). Analysis of antimicrobial whey protein-based biocomposites with lactic acid, tea tree (*Melaleuca alternifolia*) and garlic (*Allium sativum*) essential oils for Edam cheese coating. *International Journal of Dairy Technology*, 75(3), 611-618. http://dx.doi.org/10.1111/1471-0307.12858.

Wei, Z. H., & Huang, Q. R. (2020). Development of high internal phase Pickering emulsions stabilised by ovotransferrin–gum arabic particles as curcumin delivery vehicles. *International Journal of Food Science & Technology*, 55(5), 1891-1899. http://dx.doi.org/10.1111/ijfs.14340.

Wu, Y. B., Cheng, Z. X., & Huang, J. Y. (2018a). Study on the formation mechanism of soy protein isolate-chitosan complex. *He-Nong Xuebao*, 32(6), 1171-1179. http://dx.doi.org/10.11869/j.issn.100-8551.2018.06.1171.

Wu, Z. L., Zhou, F. Z., Yin, Y., & Yin, S. W. (2018b). Fabrication and characterization of stable gliadin colloid particles stabilized pickering emulsion by ultrasound. *Xiandai Shipin Keji*, 34(7), 123-127, 257. http://dx.doi.org/10.13982/j.mfst.1673-9078.2018.7.018.

Xu, Y. M., & Du, Y. M. (2003). Effect of molecular structure of chitosan on protein delivery properties of chitosan nanoparticles. *International Journal of Pharmaceutics*, 250(1), 215-226. http://dx.doi.org/10.1016/S0378-5173(02)00548-3. PMid:12480287.

Yang, H., Su, Z. W., Meng, X. H., Zhang, X. Y., Kennedy, J. F., & Liu, B. J. (2020). Fabrication and characterization of Pickering emulsion stabilized by soy protein isolate-chitosan nanoparticles. *Carbohydrate Polymers*, 247, 116712. http://dx.doi.org/10.1016/j.carbpol.2020.116712.

Yi, J., Gan, C., Wen, Z., Fan, Y., & Wu, X. (2021). Development of pea protein and high methoxyl pectin colloidal particles stabilized high internal phase pickering emulsions for p-carotene protection and delivery. *Food Hydrocolloids*, 113, 106497. http://dx.doi.org/10.1016/j.foodhyd.2020.106497.

Zhang, X., Wu, Y., Li, Y., Li, B., Pei, Y., & Liu, S. (2022). Effects of the interaction between bacterial cellulose and soy protein isolate on the oil-water interface on the digestion of the Pickering emulsions. *Food Hydrocolloids*, 126, 107480. http://dx.doi.org/10.1016/j.foodhyd.2021.107480.

Zhou, Y., Zheng, H., Yang, W., & Zhang, Q. (2020). Modification of solubility and emulsifying properties of soybean protein isolate by glycosylating with soybean oligosaccharide. *Shipin Yu Fajiao Gongye*, 46(1), 118-124. http://dx.doi.org/10.13995/j.cnki.11-1802/ts.021827.

Zhu, X. W., Chen, Y. T., Hu, Y. X., Han, Y., Xu, J. T., Zhao, Y. L., Chen, X., & Li, B. (2021). Tuning the molecular interactions between gliadin and tannic acid to prepare Pickering stabilizers with improved emulsifying properties. *Food Hydrocolloids*, 111, 106179. http://dx.doi.org/10.1016/j.foodhyd.2020.106179.